



Computational modeling of material forming processes / Simulation numérique des procédés de mise en forme

## A generalized anisotropic and asymmetric yield criterion with adjustable complexity



*Un critère d'écoulement plastique universel, anisotrope et asymétrique, avec complexité ajustable*

Christian Raemy\*, Niko Manopulo, Pavel Hora

*Institute of Virtual Manufacturing, Tannenstrasse 3, ETH Zurich, 8092 Zurich, Switzerland*

### ARTICLE INFO

#### Article history:

Received 24 August 2017

Accepted 1 March 2018

Available online 13 June 2018

#### Keywords:

Anisotropy

Strength differential

Sheet metal forming

Differential geometry

#### Mots-clés :

Anisotropie

Asymétrie traction–compression

Formage de tôle

Géométrie différentielle

### ABSTRACT

During the past decades, numerous yield criteria for orthotropic materials, possibly showing tension–compression asymmetry, were developed. Although they were applied successfully to forming simulations, they are usually only adequate for a specific class of materials. The aim of this work is to present a generalized, pressure-independent criterion for plane stress states on the base of a two-dimensional Fourier series. Its complexity is adjustable through the number of considered Fourier coefficients, and thus, albeit using an associated flow rule, virtually any number of experimental data can be captured exactly. The criterion is applicable for materials with or without tension–compression asymmetry.

© 2018 Académie des sciences. Published by Elsevier Masson SAS. All rights reserved.

### R É S U M É

Au cours des dernières décennies, de nombreux modèles de critères d'écoulement plastique ont été présentés pour décrire le comportement des matériaux orthotropes présentant éventuellement une asymétrie entre la traction et la compression. Malheureusement, ils sont, soit exclusivement applicables à une seule classe de matériaux, soit d'une grande complexité. Le but de ce travail est de développer, pour des états de contraintes planes, un modèle universel et indépendant de la pression. Le critère d'écoulement plastique proposé est basé sur une série de Fourier bidimensionnelle. La complexité du modèle étant ajustable au nombre de coefficients de Fourier considérés, la quantité de données expérimentales prise en compte est donc illimitée, et ceci même en utilisant une loi d'écoulement associée. Cette fonction permet donc de modéliser un grand nombre de matériaux différents, avec ou sans asymétrie entre la traction et la compression.

© 2018 Académie des sciences. Published by Elsevier Masson SAS. All rights reserved.

\* Corresponding author.

E-mail address: christian.raemy@ivp.mavt.ethz.ch (C. Raemy).

## 1. Introduction

Numerical simulations are nowadays indispensable for planning and optimizing forming tools and processes. The demands for better accuracy have led to the development of a vast number of constitutive material models during the past decades. Especially, numerous flow criteria were proposed for different materials, able to capture vertical and planar anisotropy and, more recently, also tension–compression asymmetry.

A first anisotropic model was proposed by Hill [1], who added flexibility to the von Mises criterion. Because of its formal simplicity and accuracy, it is still widely used today, especially for steels showing a mild anisotropy. However, it was recognized that, for instance, aluminium alloys are described more accurately by non-quadratic functions, which were firstly developed for isotropic materials, e.g., by Hosford [2], Hill [3]. Logan and Hosford [4] and Barlat and Richmond [5] used crystal plasticity simulations to provide further evidence for the suitability of non-quadratic models, Hosford [6] and Barlat and Lian [7] re-introduced anisotropy. The latter used a linear transformation of the stress tensor for this purpose, an approach that was re-adopted later by numerous authors, e.g., [8–12]. Besides the mentioned criteria that make use of generalised potential functions, some authors (e.g. [13] and [14]) proposed to re-parametrise the stress state by polar coordinates and to construct interpolation functions that describe the flow surface.

Especially materials with an *hcp* lattice show, besides anisotropy, also a tension–compression asymmetry. Asymmetric and anisotropic yield criteria were proposed by, e.g., [15–20]. Stoughton [21] proposed to decouple the yield criterion from the flow direction by the use of two different potentials and a non-associated flow rule. This, on the one hand, introduces more flexibility to the models and, on the other hand, allows for a pressure-dependent flow criterion without the prediction of plastic volume change. Several authors, such as Stoughton and Yoon [22], Bai and Wierzbicki [23], Yoon et al. [24] formulated functions for the description of tension–compression asymmetry based on this concept.

It is evident that the described multitude of flow criteria is problematic, as most functions are very specific and probably only suitable for a special class of materials. The numerical implementation into FEM code, nevertheless, is cumbersome and has to be carried out for each of those functions.

The model proposed in this work overcomes the mentioned limitations by the use of a general formulation. The stress state is re-parametrized by spherical coordinates and a two-dimensional Fourier series is applied on the angles. In that way, yield surfaces of virtually arbitrary complexity can be described. Specifically, it is straightforward to adapt the number of parameters to the number of experiments to be considered.

## 2. Proposed model

A first version of the proposed model was reported in [25], where it was applied to titanium. Here, an improved and generalized calibration procedure is presented and the important special case of materials without tension–compression asymmetry is treated.

### 2.1. Formulation of the criterion

In the space of plane stress states, the von Mises flow surface

$$\sigma_{xx}^2 - \sigma_{xx}\sigma_{yy} + \sigma_{yy}^2 + 3\tau_{xy}^2 - \sigma_y^2 = \bar{\sigma}_{vM}^2 - \sigma_y^2 = 0 \quad (1)$$

forms a (closed) ellipsoid. A natural way of describing this space is therefore the use of a periodic parametrization, which is found in a spherical coordinate system. Its zenith direction could be aligned with any of the principal axes of the ellipsoid. However, it is convenient to use the principal axis  $\{\sigma_{xx} - \sigma_{yy} = 0, \tau_{xy} = 0\}$ , the “north pole” pointing to the quadrant of biaxial compression ( $\sigma_{xx} < 0, \sigma_{yy} < 0$ ). Further, as can be seen in Fig. 1, the axes of normal stresses are scaled by a factor of  $1/\sqrt{2}$ , and the azimuthal angle  $2\psi$  is measured from the line  $\{\sigma_{xx} + \sigma_{yy} = 0, \tau_{xy} = 0\}$ , which is another principal direction of the von Mises ellipsoid (1).

In this way, there exist close relations between the loading direction  $\theta$  of a uniaxial tensile test and the coordinate  $\psi$ , and between the magnitude of stress  $\sigma$  and the radius  $r$ . This will be shown below. Analytically, the coordinate transformation reads

$$r = \sqrt{\frac{\sigma_{xx}^2}{2} + \frac{\sigma_{yy}^2}{2} + \tau_{xy}^2} \quad (2a)$$

$$\varphi = \arccos\left(-\frac{\sigma_{xx} + \sigma_{yy}}{2r}\right) \quad (2b)$$

$$\psi = \frac{1}{2} \arctan2\left(2\tau_{xy}, (\sigma_{xx} - \sigma_{yy})\right) \quad (2c)$$

with the back transformation

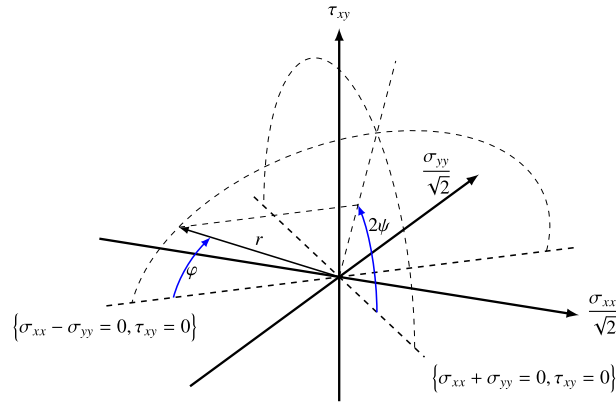


Fig. 1. Parametrization of the space of plane stress states.

$$\sigma_{xx} = r \cdot (\sin(\varphi) \cos(2\psi) - \cos(\varphi)) \tag{3a}$$

$$\sigma_{yy} = r \cdot (-\sin(\varphi) \cos(2\psi) - \cos(\varphi)) \tag{3b}$$

$$\tau_{xy} = r \cdot \sin(\varphi) \sin(2\psi) \tag{3c}$$

Applying this, von Mises equivalent stress (1) can be rewritten as

$$\begin{aligned} \bar{\sigma}_{VM}^2 &= \sigma_{xx}^2 + \sigma_{yy}^2 - \sigma_{xx}\sigma_{yy} + 3\tau_{xy}^2 \\ &= r^2 \cdot \left( \cos^2(\varphi) + 3\sin^2(\varphi) (\cos^2(2\psi) + \sin^2(2\psi)) \right) \\ &= r^2 \cdot \left( \cos^2(\varphi) + 3\sin^2(\varphi) \right) \\ &= r^2 \cdot \left( 2 - \cos(2\varphi) \right) \end{aligned} \tag{4}$$

Further, the isotropic Hosford [2] criterion

$$\bar{\sigma}_{Hosf}^a = \frac{|\sigma_1|^a + |\sigma_2|^a + |\sigma_1 - \sigma_2|^a}{2} \tag{5}$$

is, for an exponent  $a = 6$ , re-parametrized by

$$\bar{\sigma}_{Hosf}^6 = r^6 \left( \frac{25}{2} - 15 \cos(2\varphi) + \frac{9}{2} \cos(4\varphi) - \cos(6\varphi) \right) \tag{6}$$

and for  $a = 8$  by

$$\bar{\sigma}_{Hosf}^8 = r^8 \left( \frac{315}{8} - 56 \cos(2\varphi) + \frac{49}{2} \cos(4\varphi) - 8 \cos(6\varphi) + \frac{9}{8} \cos(8\varphi) \right) \tag{7}$$

Note that these criteria do not depend on the azimuthal angle  $\psi$ , as the latter is a measure of the sheet orientation. This is not the case if anisotropy is considered. For instance, the well known Hill [1] model for plane stress states

$$\bar{\sigma}_{Hill}^2 = (G + H) \sigma_{xx}^2 - 2H \sigma_{xx} \sigma_{yy} + (H + F) \sigma_{yy}^2 + 2N \tau_{xy}^2 \tag{8}$$

reads

$$\begin{aligned} \bar{\sigma}_{Hill}^2 &= r^2 \left( \frac{3F + 3G + 4H + 2N}{4} + \frac{F + G + 4H - 2N}{4} \cos(4\psi) \right. \\ &\quad + \frac{F + G - 4H - 2N}{4} \cos(2\varphi) + \frac{-F - G - 4H + 2N}{4} \cos(2\varphi) \cos(4\psi) \\ &\quad \left. + (F - G) \sin(2\varphi) \cos(2\psi) \right) \end{aligned} \tag{9}$$

In all of these examples, a two-dimensional Fourier series of the angles  $\varphi$  and  $\psi$  with the general form [26]

$$f(\varphi, \psi) := \sum_{m=0}^{\infty} \sum_{n=0}^{\infty} a_{m,n} \cos(m\varphi) \cos(n\psi) + \sum_{m=0}^{\infty} \sum_{n=1}^{\infty} b_{m,n} \cos(m\varphi) \sin(n\psi) \\ + \sum_{m=1}^{\infty} \sum_{n=0}^{\infty} c_{m,n} \sin(m\varphi) \cos(n\psi) + \sum_{m=1}^{\infty} \sum_{n=1}^{\infty} d_{m,n} \sin(m\varphi) \sin(n\psi) \quad (10)$$

can be recognized between the parentheses. The mentioned examples have fairly simple structures and, thus, compact equivalent representations. However – as stated by Dirichlet's theorem – every sufficiently continuous function can be rewritten as a (possibly infinite) Fourier series. A formally compact flow function

$$\bar{\sigma}^q = r^q f(\varphi, \psi) \quad (11)$$

is, therefore, proposed, where  $f$  is a Fourier series according to (10).

Its gradient is readily calculated as

$$\frac{\partial \bar{\sigma}}{\partial \sigma_{xx}} = P \left[ qf \frac{\sin(\varphi) \cos(2\psi) - \cos(\varphi)}{2} + \frac{\partial f}{\partial \varphi} \frac{\cos(\varphi) \cos(2\psi) + \sin(\varphi)}{2} - \frac{\partial f}{\partial \psi} \frac{\sin(2\psi)}{4 \sin(\varphi)} \right] \quad (12a)$$

$$\frac{\partial \bar{\sigma}}{\partial \sigma_{yy}} = P \left[ qf \frac{-\sin(\varphi) \cos(2\psi) - \cos(\varphi)}{2} + \frac{\partial f}{\partial \varphi} \frac{-\cos(\varphi) \cos(2\psi) + \sin(\varphi)}{2} + \frac{\partial f}{\partial \psi} \frac{\sin(2\psi)}{4 \sin(\varphi)} \right] \quad (12b)$$

$$\frac{\partial \bar{\sigma}}{\partial \tau_{xy}} = P \left[ qf \sin(\varphi) \sin(2\psi) + \frac{\partial f}{\partial \varphi} \cos(\varphi) \sin(2\psi) + \frac{\partial f}{\partial \psi} \frac{\cos(2\psi)}{2 \sin(\varphi)} \right] \quad (12c)$$

where  $P = \frac{1}{q} \left( \frac{r}{\sigma} \right)^{q-1} = \frac{1}{q} f^{\frac{1-q}{q}}$ . The gradient is thus independent of the radius, which is a consequence of the criterion being homogeneous of degree 1. Note that the partial derivatives of the series  $f$  are Fourier series themselves. They can be calculated efficiently, as the trigonometric functions already have to be evaluated for the determination of  $f$ . Further, the formal structure of the gradient is independent of the number of considered Fourier coefficients.

## 2.2. Properties

The plane stress state for a uniaxial tensile (ut) test at an angle  $\theta$  to the rolling direction with magnitude  $\sigma$  reads, in the system of orthotropy,

$$\sigma^{\text{ut}}(\theta, \sigma) = \frac{1}{2} \begin{pmatrix} 1 + \cos(2\theta) & \sin(2\theta) \\ \sin(2\theta) & 1 - \cos(2\theta) \end{pmatrix} \sigma \quad (13)$$

Applying coordinate transformation (2), the spherical coordinates

$$r^{\text{ut}}(\theta, \sigma) = \frac{\sqrt{2}}{2} \sigma \quad \varphi^{\text{ut}}(\theta, \sigma) = \frac{3\pi}{4} \quad \psi^{\text{ut}}(\theta, \sigma) = \theta \quad (14)$$

result. Thus, for uniaxial tension, the radial and polar coordinates are independent of the loading direction, while the half azimuthal angle corresponds to the angle of the loading direction. The predicted flow stress is hence

$$\sigma_{\theta}^{\text{ut}} = \frac{\sqrt{2} \sigma_y}{\sqrt[q] f \left( \frac{3\pi}{4}, \theta \right)} \quad (15)$$

Also a relatively simple expression for the tensile  $R$  values follows<sup>1</sup> from (12)

$$R_{\theta}^{\text{ut}} = - \frac{f_{,\varphi} \left( \frac{3\pi}{4}, \theta \right)}{qf \left( \frac{3\pi}{4}, \theta \right) + f_{,\varphi} \left( \frac{3\pi}{4}, \theta \right)} \quad (16)$$

<sup>1</sup> A subscript preceded by a comma denotes a partial derivative here and in the following.

The derivation of this relation is lengthy, but straightforward, and will be shown in Appendix A. Note that it is independent of the partial derivative with respect to  $\psi$ .

For uniaxial compression (uc),

$$\sigma^{uc}(\theta, \sigma) = -\sigma^{ut}(\theta, \sigma)$$

holds and therefore

$$r^{uc}(\theta, \sigma) = \frac{\sqrt{2}}{2}\sigma, \quad \varphi^{uc}(\theta, \sigma) = \frac{\pi}{4}, \quad \psi^{uc}(\theta, \sigma) = \theta - \frac{\pi}{2} \tag{17}$$

which leads to the predicted flow stress

$$\sigma_{\theta}^{uc} = \frac{\sqrt{2}\sigma_y}{\sqrt[q]{f\left(\frac{\pi}{4}, \theta - \frac{\pi}{2}\right)}} \tag{18}$$

and the predicted Lankford coefficient

$$R_{\theta}^{uc} = \frac{f_{,\varphi}\left(\frac{\pi}{4}, \theta - \frac{\pi}{2}\right)}{qf\left(\frac{\pi}{4}, \theta - \frac{\pi}{2}\right) - f_{,\varphi}\left(\frac{\pi}{4}, \theta - \frac{\pi}{2}\right)} \tag{19}$$

Equi-biaxial tension (bt) or compression (bc) with a magnitude  $\sigma$  are characterized by the plane stress states

$$\sigma^{bt}(\sigma) = \begin{pmatrix} 1 & 0 \\ 0 & 1 \end{pmatrix} \sigma \quad \sigma^{bc}(\sigma) = -\begin{pmatrix} 1 & 0 \\ 0 & 1 \end{pmatrix} \sigma \tag{20}$$

which leads to

$$r^{bt}(\sigma) = \sigma, \quad \varphi^{bt}(\sigma) = \pi \tag{21a}$$

$$r^{bc}(\sigma) = \sigma, \quad \varphi^{bc}(\sigma) = 0 \tag{21b}$$

and an undetermined value of  $\psi$ . This ambiguity is due to the singularity of the parametrization and will be treated later. Setting  $\psi = 0$ , the predicted equi-biaxial flow stresses read

$$\sigma^{bt} = \frac{\sigma_y}{\sqrt[q]{f(\pi, 0)}}, \quad \sigma^{bc} = \frac{\sigma_y}{\sqrt[q]{f(0, 0)}} \tag{22}$$

and the predicted biaxial “R values” defined as

$$R^{bt/c} = \frac{d\varepsilon_{yy}^p}{d\varepsilon_{xx}^p} \tag{23}$$

are

$$R^{bt} = \left. \frac{qf + f_{,\varphi}}{qf - f_{,\varphi}} \right|_{\varphi=\pi, \psi=0}, \quad R^{bc} = \left. \frac{qf + f_{,\varphi}}{qf - f_{,\varphi}} \right|_{\varphi=0, \psi=0} \tag{24}$$

Simple shear (ss), characterized by a tensile stress acting at an angle  $\theta$  to the rolling direction with magnitude  $\sigma$  and compressive stress acting in the perpendicular direction with the same magnitude, leads to the stress state

$$\sigma^{ss}(\theta, \sigma) = \begin{pmatrix} \cos(2\theta) & \sin(2\theta) \\ \sin(2\theta) & -\cos(2\theta) \end{pmatrix} \sigma \tag{25}$$

in global coordinates. This translates to

$$r^{ss}(\theta, \sigma) = \sigma, \quad \varphi^{ss}(\theta, \sigma) = \frac{\pi}{2}, \quad \psi^{ss}(\theta, \sigma) = \theta \tag{26}$$

again with constant radius and polar coordinates and the half azimuthal angle corresponding to the loading direction. Thus, the predicted flow stress under shear reads

$$\sigma_{\theta}^{ss} = \frac{\sigma_y}{\sqrt[q]{f\left(\frac{\pi}{2}, \theta\right)}} \tag{27}$$

A tensile stress state leading to a plane strain (pst) state is characterized by a tensile principal stress with magnitude  $\sigma_1$  acting at an angle  $\theta$  to the rolling direction and a perpendicular tensile principal stress with magnitude  $\sigma_2$ . In the global coordinate system, the corresponding tensor components read

$$\sigma^{\text{pst}}(\theta, \sigma_1, \sigma_2) = \frac{1}{2} \begin{pmatrix} \sigma_1 [1 + \cos(2\theta)] + \sigma_2 [1 - \cos(2\theta)] & (\sigma_1 - \sigma_2) \sin(2\theta) \\ (\sigma_1 - \sigma_2) \sin(2\theta) & \sigma_1 [1 - \cos(2\theta)] + \sigma_2 [1 + \cos(2\theta)] \end{pmatrix} \quad (28)$$

The transformation to the spherical coordinates yields

$$r^{\text{pst}}(\theta, \sigma_1, \sigma_2) = \sqrt{\frac{\sigma_1^2 + \sigma_2^2}{2}}, \quad \varphi^{\text{pst}}(\theta, \sigma_1, \sigma_2) = \arccos\left(-2 \frac{\sigma_1 + \sigma_2}{r^{\text{pst}}(\theta, \sigma_1, \sigma_2)}\right), \quad \psi^{\text{pst}}(\theta, \sigma_1, \sigma_2) = \theta \quad (29)$$

Further, the plane strain condition (vanishing transversal strain in the local coordinate system) also dictates the value of the partial derivative  $f_{,\varphi}$

$$f_{,\varphi}(\varphi^{\text{pst}}, \theta) = qf(\varphi^{\text{pst}}, \theta) \frac{\sin(\varphi^{\text{pst}}) + \cos(\varphi^{\text{pst}})}{\sin(\varphi^{\text{pst}}) - \cos(\varphi^{\text{pst}})} \quad (30)$$

The derivation of this result can be found in Appendix B.

These relations can be used to calibrate the model (see below), if the positions of the plane strain points are known from experiments. On the other hand – as with many other flow functions – it is not straightforward to determine the *predicted* plane strain points, as a non-linear system of equations has to be solved.

### 2.3. Physical considerations

The proposed criterion (11) allows for virtually arbitrarily shaped flow surfaces in the space of plane stresses. However, some physical constraints must be enforced when applied to sheet metal.

- The function has to be orthotropic, i.e. symmetric with respect to the plane  $\tau_{xy} = 0$ . In terms of the spherical coordinates this means  $f$  must be an even function of  $\psi$ . Therefore, only cosine terms of  $\psi$  are allowed for the construction of the series

$$b_{m,n} = d_{m,n} = 0 \quad \forall \{m, n\} \quad (31)$$

- The surface obviously must be closed. Because the azimuthal angle is defined as  $2\psi$ , the series  $f$  has to be a periodic function of  $\psi$  with a period of  $4\pi$ . Hence, only even-numbered multiples of  $\psi$  must occur in  $f$  or

$$a_{m,n} = c_{m,n} = 0 \quad \text{if } n \text{ is odd} \quad (32)$$

- Singularities, which are inherent to spherical coordinates, lead to an ambiguity of the azimuthal angle at the poles. Consequently, the value of  $f$  should be same for all  $\psi$  at these positions. Or, put differently, the partial derivative with respect to the azimuthal angle must vanish at the poles

$$f_{,\psi}(\pi, \psi) = 0 \quad \forall \psi \quad (33a)$$

$$f_{,\psi}(0, \psi) = 0 \quad \forall \psi \quad (33b)$$

In that way, also the singularities that occur in the gradient (12) become removable.

- The constraints (33a) and (33b) prevent “jumps” of the surface at the poles. But also its tangent, which is represented here by the derivative of  $f$  w.r.t.  $\varphi$ , should be continuous. This is ensured by the constraints

$$f_{,\varphi}(\pi, \psi) = -f_{,\varphi}(\pi, \psi + \pi/2) \quad \forall \psi \quad (34a)$$

$$f_{,\varphi}(0, \psi) = -f_{,\varphi}(0, \psi + \pi/2) \quad \forall \psi \quad (34b)$$

- In the important case of a material without tension–compression asymmetry, the function must return the same value for the stress states  $\{\sigma_{xx}, \sigma_{yy}, \tau_{xy}\}$  and  $\{-\sigma_{xx}, -\sigma_{yy}, \tau_{xy}\}$  (symmetry in  $\tau_{xy}$  is already fulfilled through orthotropy). If former stress state is denoted by a superscript + and latter by a superscript –, this translates to

$$r^- = r^+, \quad \varphi^- = \pi - \varphi^+, \quad \psi^- = \frac{\pi}{2} - \psi^+ \quad (35)$$

in spherical coordinates, thus  $f(\varphi, \psi) = f(\pi - \varphi, \frac{\pi}{2} - \psi)$  is required. From this,

$$a_{m,n} = 0 \quad \text{if } \{m \text{ is even and } n/2 \text{ is odd}\} \text{ or } \{m \text{ is odd and } n/2 \text{ is even}\} \quad (36a)$$

$$c_{m,n} = 0 \quad \text{if } \{m \text{ is even and } n/2 \text{ is even}\} \text{ or } \{m \text{ is odd and } n/2 \text{ is odd}\} \quad (36b)$$

follows.

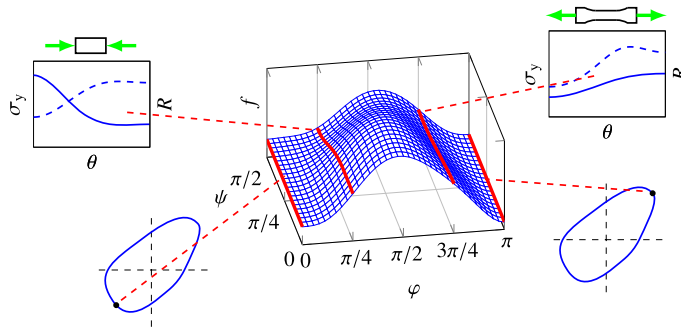


**Fig. 2.** Visualisation of the parameter identification procedure. One-dimensional Fourier series (red solid lines) are constructed based on experimental data. A two dimensional series  $f$ , spanned by the sub-series, is sought such that a convex flow surface results. Here, uniaxial and equibiaxial tests are considered; further one-dimensional support functions could be obtained through plane strain and/or simple shear experiments.

**2.4. Calibration**

The parameter identification procedure is rather different from other flow criteria. Instead of minimising the error between the predicted and the measured values of flow stresses and Lankford coefficients, the Fourier coefficients are optimised so that a convex flow surface results while the physical restrictions and experimental data impose constraints on the optimisation problem. Expressed more figuratively, one-dimensional Fourier sub-series are constructed based on experimental data, and the two-dimensional series  $f$ , spanned by the sub-series, is sought such that a convex flow surface results. This concept is visualised in Fig. 2.

Convexity is assessed by means of the Gaussian curvature  $K$  of the flow surface, which is determined for a sample of 1681 points ( $41 \times 41$ ) of the parameter space  $\{\varphi \in [0, \pi], \psi \in [0, \pi/2]\}$ . If all curvatures are positive, the surface is assumed to be strictly convex. This procedure is no proof in the mathematical sense. However, according to the Nyquist–Shannon sampling theorem, the chosen sample is sufficient to analyse a series containing harmonics up to the 20th order in  $\varphi$  and 40th order in  $\psi$ . As it will be shown below, only frequencies well below these values are usually necessary and, therefore, it is unlikely that a non-convex area of the yield surface remains undetected. Increasing the sample, on the other hand, does not add further information, but leads to longer calculation times during the fitting procedure.

The objective function

$$Err = - \min_i (K_i) \tag{37}$$

where the index  $i$  runs over all samples, is hence minimized by varying the Fourier coefficients. The optimization was carried out by use of the `fminimax` function of *MATLAB® R2017b Optimization Toolbox™*. This algorithm reformulates the problem into an equivalent non-linear programming problem which is solved by a sequential quadratic programming method. As – in most cases – more Fourier coefficients than experimental data are needed to allow for a convex flow surface, the solution is in general not unique and dependent on the start values.

The Gaussian curvature is computed through the relation

$$K = \frac{\alpha\beta - \gamma^2}{AB - \Gamma^2} \tag{38}$$

where  $A, B, \Gamma, \alpha, \beta$  and  $\gamma$  are the coefficients of the first and second fundamental form [27]

$$\begin{pmatrix} A & \Gamma \\ \Gamma & B \end{pmatrix} = \begin{pmatrix} \mathbf{x}_{,\varphi} \cdot \mathbf{x}_{,\varphi} & \mathbf{x}_{,\varphi} \cdot \mathbf{x}_{,\psi} \\ \mathbf{x}_{,\psi} \cdot \mathbf{x}_{,\varphi} & \mathbf{x}_{,\psi} \cdot \mathbf{x}_{,\psi} \end{pmatrix}, \quad \begin{pmatrix} \alpha & \gamma \\ \gamma & \beta \end{pmatrix} = \begin{pmatrix} \mathbf{v} \cdot \mathbf{x}_{,\varphi\varphi} & \mathbf{v} \cdot \mathbf{x}_{,\varphi\psi} \\ \mathbf{v} \cdot \mathbf{x}_{,\psi\varphi} & \mathbf{v} \cdot \mathbf{x}_{,\psi\psi} \end{pmatrix}, \quad \mathbf{v} = \frac{\mathbf{x}_{,\varphi} \times \mathbf{x}_{,\psi}}{\|\mathbf{x}_{,\varphi} \times \mathbf{x}_{,\psi}\|} \tag{39}$$

with  $\mathbf{v}$  representing the normalized outward normal and  $\mathbf{x}(\varphi, \psi)$  the explicit parametrisation of the yield surface, which is obtained by rearranging (11) to

$$\mathbf{x}(\varphi, \psi) = \begin{pmatrix} \sigma_{xx} \\ \sigma_{yy} \\ \tau_{xy} \end{pmatrix} = \frac{\sigma_y}{\sqrt[3]{f(\varphi, \psi)}} \cdot \begin{pmatrix} \sin(\varphi) \cos(2\psi) - \cos(\varphi) \\ -\sin(\varphi) \cos(2\psi) - \cos(\varphi) \\ \sin(\varphi) \sin(2\psi) \end{pmatrix} \tag{40}$$

The optimisation is subject to the following constraints.

- Orthotropy is guaranteed if conditions (31) and (32) are fulfilled. It is convenient to remove the corresponding coefficients *before* the actual calibration procedure, as it significantly reduces the number of design variables.
- If no tension–compression asymmetry has to be considered, further coefficients can be removed through (36).

- To remove the effects of the singularities, (33) and (34) have to be enforced. To this end, (33a) is expanded

$$f_{,\psi}(\pi, \psi) = \sum_m \sum_n \frac{\partial}{\partial \psi} [a_{m,n} \cos(m\pi) \cos(n\psi) + c_{m,n} \sin(m\pi) \cos(n\psi)] \equiv 0 \quad \forall \psi$$

and

$$\sum_m a_{m,n} (-1)^m = 0, \quad n = 2, 4, \dots \quad (41)$$

follows. Similarly for (33a), it follows from

$$f_{,\psi}(0, \psi) = \sum_m \sum_n \frac{\partial}{\partial \psi} [a_{m,n} \cos(0) \cos(n\psi) + c_{m,n} \sin(0) \cos(n\psi)] \equiv 0 \quad \forall \psi$$

the constraint

$$\sum_m a_{m,n} = 0, \quad n = 2, 4, \dots \quad (42)$$

The relation corresponding to (34a) is slightly more complex. Expanding leads to

$$\begin{aligned} 0 &= f_{,\varphi}(\pi, \psi) + f_{,\varphi}(\pi, \psi + \pi/2) \\ &= \sum_m \sum_n m \left[ -a_{m,n} \sin(m\pi) (\cos(n\psi) + \cos(n\psi + n\pi/2)) + c_{m,n} \cos(m\pi) (\cos(n\psi) + \cos(n\psi + n\pi/2)) \right] \\ &= \sum_m \sum_n m c_{m,n} (-1)^m \left( \cos(n\psi) - \sin(n\psi) \sin\left(\frac{n}{2}\pi\right) + \cos(n\psi) \cos\left(\frac{n}{2}\pi\right) \right) \\ &= \sum_m \sum_n m c_{m,n} (-1)^m \left( 1 + (-1)^{n/2} \right) \cos(n\psi), \quad \forall \psi \end{aligned}$$

and hence

$$\sum_m m c_{m,n} (-1)^m \left( 1 + (-1)^{n/2} \right) = 0, \quad n = 0, 2, 4, \dots \quad (43)$$

Finally, for (34b)

$$\begin{aligned} 0 &= f_{,\varphi}(0, \psi) + f_{,\varphi}(0, \psi + \pi/2) \\ &= \sum_m \sum_n m \left[ -a_{m,n} \sin(0) (\cos(n\psi) + \cos(n\psi + n\pi/2)) + c_{m,n} \cos(0) (\cos(n\psi) + \cos(n\psi + n\pi/2)) \right] \\ &= \sum_m \sum_n m c_{m,n} \left( 1 + (-1)^{n/2} \right) \cos(n\psi), \quad \forall \psi \end{aligned}$$

and thus

$$\sum_m m c_{m,n} \left( 1 + (-1)^{n/2} \right) = 0, \quad n = 0, 2, 4, \dots \quad (44)$$

- Biaxial flow stresses are captured by rearranging (22)

$$f(\pi, 0) = \sum_m \sum_n a_{m,n} (-1)^m = \left( \frac{\sigma_y}{\sigma^{bc}} \right)^q \quad (45a)$$

$$f(0, 0) = \sum_m \sum_n a_{m,n} = \left( \frac{\sigma_y}{\sigma^{bc}} \right)^q \quad (45b)$$

- Biaxial  $R$  values can be set by rearranging (24)

$$f_{,\varphi}(\pi, 0) = \sum_m \sum_n m c_{m,n} (-1)^m = q f(\pi, 0) \frac{R^{bc} - 1}{R^{bc} + 1} = q \left( \frac{\sigma_y}{\sigma^{bc}} \right)^q \frac{R^{bc} - 1}{R^{bc} + 1} \quad (46a)$$

$$f_{,\varphi}(0, 0) = \sum_m \sum_n m c_{m,n} = q f(0, 0) \frac{R^{bc} - 1}{R^{bc} + 1} = q \left( \frac{\sigma_y}{\sigma^{bc}} \right)^q \frac{R^{bc} - 1}{R^{bc} + 1} \quad (46b)$$

- A major advantage of the proposed criterion is the procedure for capturing uniaxial flow stresses and  $R$  values. If necessary, any number of experiments can be captured accurately by adding non-zero Fourier coefficients to  $f$ . To this end, one-dimensional series are assembled based on the experimental data, and by means of constraints,  $f$  is forced to follow them (Fig. 2). If – as an example – tensile uniaxial flow stresses were measured in three directions,  $\theta = \{0^\circ, 45^\circ, 90^\circ\}$  to the rolling direction, a Fourier series

$$g^{ut}(\theta) = \sum_n g_n^{ut} \cos(n\theta) = g_0^{ut} + g_2^{ut} \cos(2\theta) + g_4^{ut} \cos(4\theta)$$

with three coefficients is required. The coefficients can be calculated by solving the linear system of equations

$$\begin{pmatrix} 1 & \cos(0) & \cos(0) \\ 1 & \cos(\pi/2) & \cos(\pi) \\ 1 & \cos(\pi) & \cos(2\pi) \end{pmatrix} \begin{pmatrix} g_0^{ut} \\ g_2^{ut} \\ g_4^{ut} \end{pmatrix} = \begin{pmatrix} \left(\frac{\sqrt{2}\sigma_y}{\sigma_{0^\circ}^{ut}}\right)^q \\ \left(\frac{\sqrt{2}\sigma_y}{\sigma_{45^\circ}^{ut}}\right)^q \\ \left(\frac{\sqrt{2}\sigma_y}{\sigma_{90^\circ}^{ut}}\right)^q \end{pmatrix} \tag{47}$$

which follows from rearranging (15). The flow function can be forced to reproduce the measurements exactly by setting

$$f\left(\frac{3\pi}{4}, \theta\right) = g^{ut}(\theta) \tag{48}$$

thus by the constraints

$$\sum_m \left[ a_{m,n} \cos\left(m\frac{3\pi}{4}\right) + c_{m,n} \sin\left(m\frac{3\pi}{4}\right) \right] = g_n^{ut}, \quad n = 0, 2, 4, \dots \tag{49}$$

For compression, a series  $g^{uc}(\psi)$  is constructed analogously as above and

$$f\left(\frac{\pi}{4}, \psi\right) = g^{uc}(\psi) = \sum_n g_n^{uc} \cos\left(n\left(\theta - \frac{\pi}{2}\right)\right)$$

is enforced by the constraints

$$\sum_m \left[ a_{m,n} \cos\left(m\frac{\pi}{4}\right) + c_{m,n} \sin\left(m\frac{\pi}{4}\right) \right] = g_n^{uc}, \quad n = 0, 2, 4, \dots \tag{50}$$

Note that any number of experiments (angles to the rolling direction) could be captured. However, to prevent over-fitting, the experimental data can also be mapped in a least-square sense by considering less coefficients in the series  $g^{ut}$  and  $g^{uc}$ . In that case, the coefficients can be found by solving the system of equations

$$\mathbf{A}^T \mathbf{A} \begin{pmatrix} g_0^{ut/c} \\ \vdots \\ g_n^{ut/c} \end{pmatrix} = \mathbf{A}^T \mathbf{b} \tag{51}$$

if  $\mathbf{A}$  is the coefficient matrix and  $\mathbf{b}$  the right-hand-side in (47).

- Uniaxial  $R$  values are treated in a similar manner. For tension, a one-dimensional Fourier series

$$h^{ut}(\theta) = \sum_n h_n^{ut} \cos(n\theta) = -qf\left(\frac{3\pi}{4}, \theta\right) \frac{R_\theta^{ut}}{R_\theta^{ut} + 1} = -qg^{ut}(\theta) \frac{R_\theta^{ut}}{R_\theta^{ut} + 1} \tag{52}$$

is constructed following from (16) and

$$f_{,\varphi}\left(\frac{3\pi}{4}, \theta\right) = h^{ut}(\theta) \tag{53}$$

is enforced via the constraints

$$\sum_m \left[ -ma_{m,n} \sin\left(m\frac{3\pi}{4}\right) + mc_{m,n} \cos\left(m\frac{3\pi}{4}\right) \right] = h_n^{ut}, \quad n = 0, 2, 4, \dots \tag{54}$$

In the case of uniaxial compression, the one-dimensional series is obtained by rearranging (19)

$$h^{uc}(\psi) = \sum_n h_n^{uc} \cos\left(n\left(\theta - \frac{\pi}{2}\right)\right) = qf\left(\frac{\pi}{4}, \theta - \frac{\pi}{2}\right) \frac{R_\theta^{uc}}{R_\theta^{uc} + 1} = qg^{uc}\left(\theta - \frac{\pi}{2}\right) \frac{R_\theta^{uc}}{R_\theta^{uc} + 1} \quad (55)$$

and

$$f_{,\varphi}\left(\frac{\pi}{4}, \psi\right) = h^{uc}(\psi) \quad (56)$$

leads to the constraints

$$\sum_m \left[ -ma_{m,n} \sin\left(m\frac{\pi}{4}\right) + mc_{m,n} \cos\left(m\frac{\pi}{4}\right) \right] = h_n^{uc}, \quad n = 0, 2, 4, \dots \quad (57)$$

### 3. Applications and discussion

The proposed criterion was initially developed for a commercially pure titanium sheet [25], which shows a pronounced tension–compression asymmetry. Only three loading directions were considered there. It will now be shown that the model is easily applicable also to materials without tension–compression asymmetry. The necessary amount of Fourier coefficients for an accurate description of a higher number of experimental data will be discussed.

The implementation of the criterion into finite element software is not considered here. However, current numerical techniques for stress updating are compatible with the proposed model, as it was shown in [25], where a convex cutting plane algorithm [28] was used, and in [29] by using a closest point projection algorithm [28].

#### 3.1. Aluminium alloy without strength differential

As an example of a material with rather complex properties, but not showing tension–compression asymmetry, the aluminium alloy AA2090-T3 is considered. Its properties were reported by Park and Chung [30], who used the yld2000-2d model [9] and a non-associated flow rule to capture the experimental data. The uniaxial flow stresses of seven directions (0°, 15°, 30°, 45°, 60°, 75° and 90°) and the corresponding Lankford coefficients as well as the biaxial flow stress and the  $R$  value were indicated, thus a total of 16 measurements.

The proposed model was calibrated to the reported data by the procedure outlined above. A varying number of non-zero coefficients of  $f$  was applied in the  $\psi$  direction. The number of coefficients in the  $\varphi$  direction was increased successively until convex solutions could be found in all cases, leading to a total of 13 harmonics in the  $\varphi$  direction; one constant and 6 cosine and sine terms, respectively,  $q = 6$ . The predicted yield loci are presented in Fig. 3a; the courses of uniaxial flow stress and Lankford coefficients of the differently calibrated models are displayed in Figs. 3b and 3c.

It is observed that the measured flow stress as well as  $R$  values show significant oscillations. Specifically, in the 45° direction a relatively low flow stress, but quite elevated  $R$  value is exhibited by the material.

The proposed model captures exactly both biaxial flow stress and  $R$  values (those constraints were enforced for all number of Fourier coefficients). With an increasing number of Fourier coefficients, also the predictions of the uniaxial data get progressively more accurate. With only one coefficient in the  $\psi$  direction, the values are clearly constant and reflect an average<sup>2</sup> flow stress and  $R$  value. With a bipartite series, the general trends are mapped and with four coefficients in the  $\psi$  direction, already a rather accurate approximation is obtained, at least for the flow stresses. Lankford coefficients are captured less precisely because of the “outlier” at 45°. Using five harmonics, the approximation is improved significantly, except for the region around 15° to the rolling direction. With six harmonics in the  $\psi$  direction, almost exact predictions are obtained (the corresponding coefficients for this case are given in Appendix C), seven harmonics finally reproduce the exact values. It is important to highlight the fact that, because of the high number of necessary harmonics in the  $\varphi$  direction, every added harmonic in the  $\psi$  direction significantly increases the total number of Fourier coefficients – the chosen parameter set in Appendix C contains 39 coefficients. Thus, the user has to make a trade-off between accuracy and a lightweight data set.

The different predicted flow stresses and Lankford coefficients are also reflected in the yield loci. While the predictions of the first and third quadrant are similar for all variants, the predicted strength under pure shear varies significantly, since it is strongly influenced by the slope of the curve at the uniaxial points. As seen above, also the shape of this region could be calibrated if corresponding experimental data were present.

Note that the least-square fit of the  $R$  values has led to negative predicted values if three harmonics were considered. Consequently, no convex flow surface could be found in this situation. However, a model with three harmonics could be calibrated straightforwardly by considering only experiments in 0°, 45° and 90° directions, in which case the model predicts also the exact values at these positions. The error at the other angles, nevertheless, is significant. Most state-of-the-art models also only consider those three directions, and thus similar differences can be expected. Because of the complexity

<sup>2</sup> It is not an average in the usual sense, as it can be seen in equation (47).

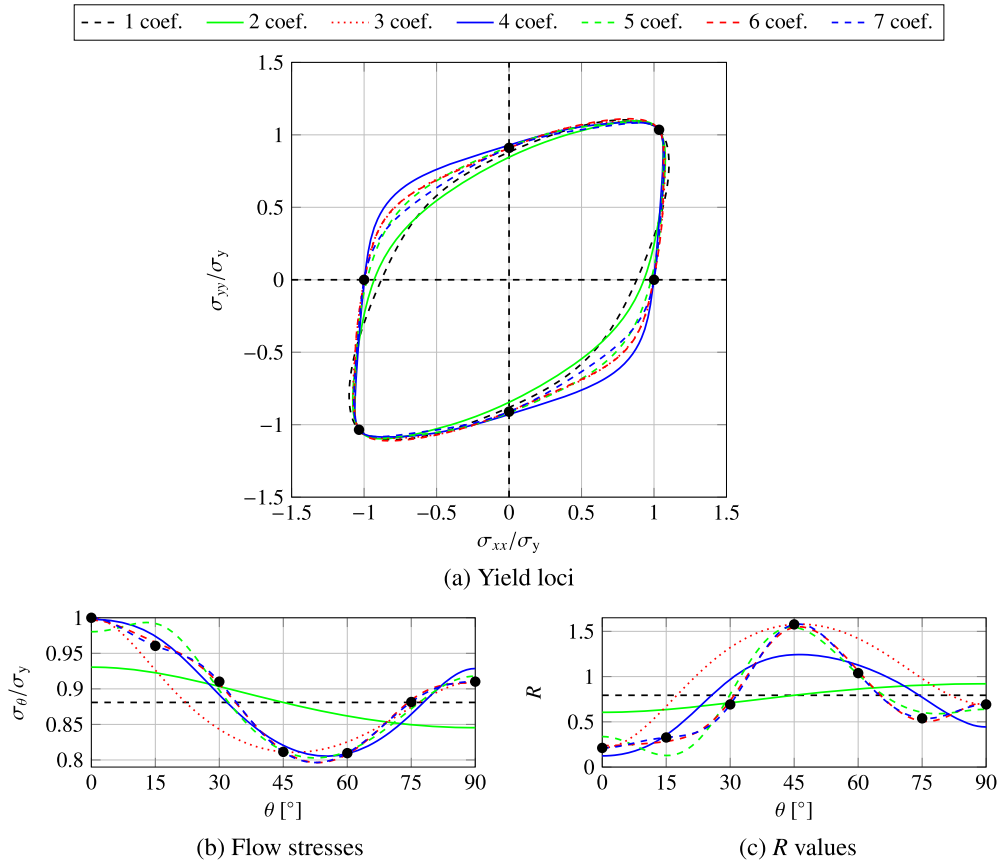


**Fig. 3.** Predicted yield loci, uniaxial flow stresses and R values for AA2090 (experimental data taken from [30]), with different numbers of Fourier coefficients in the  $\psi$  direction.

of the material characteristics, it is therefore advised to use the proposed model with six or seven harmonics in the  $\psi$  direction.

### 3.2. Aluminium alloy showing strength differential

The ability of the flow function to model a complex material that exhibits a strength differential effect is demonstrated on aluminium AA2008-T4. Its properties were reported by Yoon et al. [31]. They indicated tensile and compressive uniaxial flow stresses in seven directions, tensile uniaxial R values, and biaxial flow stresses, thus 22 data in sum. Because of the lack of compressive R values, they were assumed to be equal to their tensile counterpart. Stoughton and Yoon [22], who modelled the same material, implicitly made the same assumption. They used a non-associated flow rule with a pressure-dependent yield criterion and a symmetric flow potential. Although it would not be necessary to impose constraints on the compressive R values for the proposed model, they were nonetheless considered in order to demonstrate flexibility. Further, as biaxial compressive flow stress was not indicated, it was assumed that the strength-differential ratio of the biaxial flow stresses is the same as the average ratio of the uniaxial flow stresses. Biaxial R values were not indicated either, they were assumed to have the isotropic value 1.

The model was again calibrated with different numbers of non-vanishing Fourier coefficients in the  $\psi$  direction, while the number in the  $\varphi$  direction was kept constant. Compared to AA2090-T3, less Fourier coefficients (one constant and four cosine and sine terms, respectively,  $q = 2$ ) in the  $\varphi$  direction were needed to obtain a convex solution, as the yield loci show less sharp corners.<sup>3</sup> The different approximations of the experimental data are shown in Fig. 4.

In contrast to the previous example, the measured properties of this material follow rather smooth curves, except for the compressive flow stress at 60°. Due to this, quite accurate approximations are already feasible with a low number of Fourier coefficients in the  $\psi$  direction. However, with two harmonics, the approximation of the predicted compressive flow stresses

<sup>3</sup> It is known from Fourier analysis that a signal with “sharp” transitions contains high-frequency components.

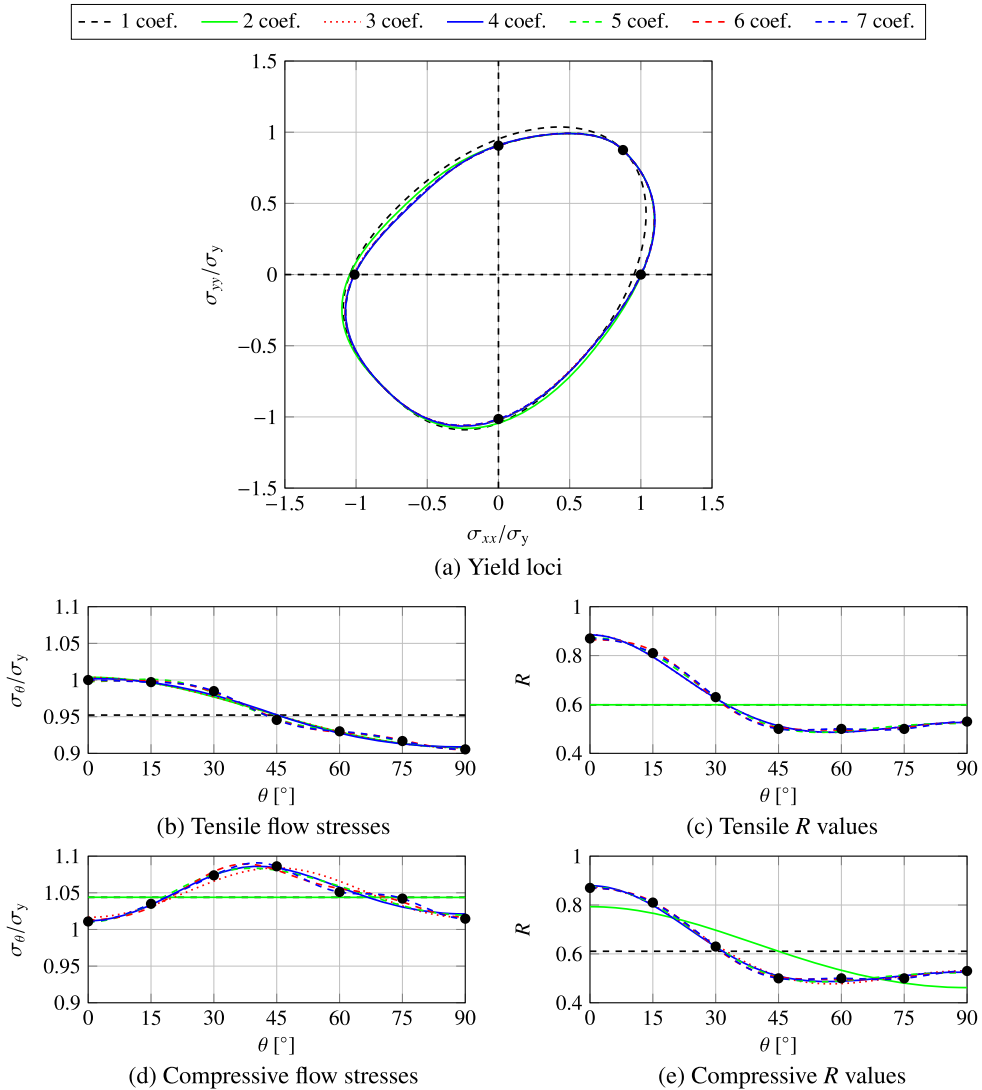


**Fig. 4.** Predicted yield loci, uniaxial flow stresses and  $R$  values for AA2008-T4 (experimental data taken from [31]), with different numbers of Fourier coefficients in the  $\psi$  direction.

are almost constant, because the measurements show a mirror symmetry at  $45^\circ$ , while the other measurements only have symmetries around  $0^\circ$  and  $90^\circ$ .<sup>4</sup>

The predictions are virtually identical for three to seven harmonics in the  $\psi$  direction. An exact mapping of the measurements – especially of the compressive flow stress at  $60^\circ$  – requires all seven harmonics. However, the measurement of flow stresses is subject to some uncertainties, and thus the mentioned experimental point might contain a small error. Consequently, there is a risk of over-fitting if an approximation with seven harmonics is applied. It is therefore recommended to use only three harmonic parameters (details are given in Appendix C) for this material – in contrast to AA2090, where at least six harmonics were necessary to get sufficiently accurate approximations.

#### 4. Conclusions

A yield criterion for plane stress states with a very compact, yet flexible formulation was presented. As it is based on a Fourier series, its complexity can be adapted to the desired degree by adding or removing Fourier coefficients. This means, although an associated flow rule is used, a high number of experimental data can be reproduced exactly. On the other hand, the data can be approximated in a least square sense by a simpler series. In this case, a very smooth flow surface results.

<sup>4</sup> This means that the compressive flow stresses follow roughly a cosine wave with a period of  $\pi/2$ , the other experiments a cosine wave with a period of  $\pi$ . Note that only cosines of even-numbered multiples of  $\psi$  are allowed. Hence, a bipartite series consists of a constant term and a cosine with period  $\pi$ .

Any intermediate configuration can be realised. Nevertheless, the formal structure of the flow function and its derivatives remain unchanged.

**Appendix A. Derivation of the predicted Lankford parameters**

An associated flow rule

$$d\epsilon_{ij}^{p,ut} = d\bar{\epsilon}^p \frac{\partial \bar{\sigma}}{\partial \sigma_{ij}} \tag{58}$$

is assumed in the following derivations and argument lists are omitted where appropriate.

The stress state for a uniaxial tensile test is characterized by the spherical coordinates (14), incremental plastic strain thus reads

$$\frac{d\epsilon_{xx}^{p,ut}}{d\bar{\epsilon}^p} = \frac{f^{\frac{1-q}}{q}}{q} \frac{\sqrt{2}}{2} \left[ qf \frac{1 + \cos(2\theta)}{2} + f_{,\varphi} \frac{1 - \cos(2\theta)}{2} - f_{,\psi} \frac{\sin(2\theta)}{2} \right] \tag{59a}$$

$$\frac{d\epsilon_{yy}^{p,ut}}{d\bar{\epsilon}^p} = \frac{f^{\frac{1-q}}{q}}{q} \frac{\sqrt{2}}{2} \left[ qf \frac{1 - \cos(2\theta)}{2} + f_{,\varphi} \frac{1 + \cos(2\theta)}{2} + f_{,\psi} \frac{\sin(2\theta)}{2} \right] \tag{59b}$$

$$\frac{d\epsilon_{xy}^{p,ut}}{d\bar{\epsilon}^p} = \frac{f^{\frac{1-q}}{q}}{2q} \frac{\sqrt{2}}{2} \left[ qf \sin(2\theta) - f_{,\varphi} \sin(2\theta) + f_{,\psi} \cos(2\theta) \right] \tag{59c}$$

Note that  $d\epsilon_{xy}^{p,ut} = \frac{1}{2} d\gamma_{xy}^{p,ut} = \frac{1}{2} \frac{\partial \bar{\sigma}}{\partial \tau_{xy}}$ . This tensor can be represented by a sum of three matrices

$$\begin{aligned} \sqrt{2} q f^{\frac{q-1}{q}} \frac{d\mathbf{\epsilon}^{p,ut}}{d\bar{\epsilon}^p} &= qf \underbrace{\begin{pmatrix} \cos^2(\theta) & \frac{1}{2} \sin(2\theta) \\ \frac{1}{2} \sin(2\theta) & \sin^2(\theta) \end{pmatrix}}_{=:A} \\ &+ f_{,\varphi} \underbrace{\begin{pmatrix} \sin^2(\theta) & -\frac{1}{2} \sin(2\theta) \\ -\frac{1}{2} \sin(2\theta) & \cos^2(\theta) \end{pmatrix}}_{=:B} + \frac{1}{2} f_{,\psi} \underbrace{\begin{pmatrix} -\sin(2\theta) & \cos(2\theta) \\ \cos(2\theta) & \sin(2\theta) \end{pmatrix}}_{=:C} \end{aligned} \tag{60}$$

For a uniaxial tensile test, the *R* values are defined as  $R = \frac{d\epsilon_{width}^p}{d\epsilon_{thickness}^p}$ , which corresponds to  $R = \frac{d\epsilon_{yy}^p}{d\epsilon_{zz}^p}$  in a coordinate system where the *x* axis is aligned with the loading direction. The incremental plastic strain (60) must thus be rotated to the local coordinate system by means of the rotation matrix

$$\mathbf{R}_\theta = \begin{pmatrix} \cos(\theta) & \sin(\theta) \\ -\sin(\theta) & \cos(\theta) \end{pmatrix} \tag{61}$$

with

$$\mathbf{R}_\theta \mathbf{A} \mathbf{R}_\theta^T = \begin{pmatrix} 1 & 0 \\ 0 & 0 \end{pmatrix} \quad \mathbf{R}_\theta \mathbf{B} \mathbf{R}_\theta^T = \begin{pmatrix} 0 & 0 \\ 0 & 1 \end{pmatrix} \quad \mathbf{R}_\theta \mathbf{C} \mathbf{R}_\theta^T = \begin{pmatrix} 0 & 1 \\ 1 & 0 \end{pmatrix} \tag{62}$$

the incremental plastic strain in the local coordinate system follows

$$\sqrt{2} q f^{\frac{1-q}{q}} \frac{d\mathbf{\epsilon}^{p,ut,local}}{d\bar{\epsilon}^p} = \begin{pmatrix} qf & \frac{1}{2} f_{,\psi} \\ \frac{1}{2} f_{,\psi} & f_{,\varphi} \end{pmatrix} \tag{63}$$

Applying plastic volume constancy  $d\epsilon_{zz}^p = -d\epsilon_{xx}^p - d\epsilon_{yy}^p$ , one finds

$$R_\theta^{ut} = - \frac{f_{,\varphi} \left( \frac{3\pi}{4}, \theta \right)}{qf \left( \frac{3\pi}{4}, \theta \right) + f_{,\varphi} \left( \frac{3\pi}{4}, \theta \right)} \tag{64}$$

The procedure is similar for uniaxial compression.

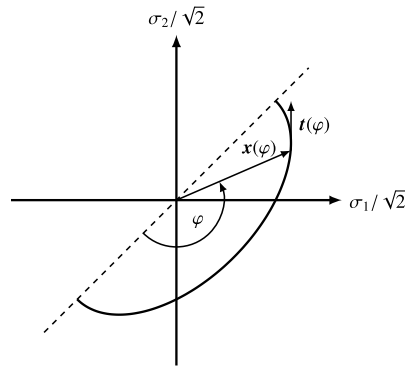


**Fig. B.5.** Cut of the flow surface through the half plane  $\psi = \theta$  in modified stress space with local system of coordinates and tangential vector to the yield locus.

### Appendix B. Derivation of $f_{,\varphi}$ at the plane strain points

To obtain the partial derivatives  $f_{,\varphi}$  at the plane strain points, we think of the half plane  $\psi = \theta$  in the modified stress space. In Fig. 1, this half plane is spanned by the half circle in which the position vector lies. A local system of coordinates is assigned to the plane, where the first base vector points to the direction of the principal tensile stress  $\sigma_1$ , and the second base vector to the direction of  $\sigma_2$ , see Fig. B.5.

In accordance to (3), a position vector  $\mathbf{x}$  on this manifold may be parametrized as

$$\mathbf{x} = r \underbrace{\begin{pmatrix} \sin(\varphi) - \cos(\varphi) \\ -\sin(\varphi) - \cos(\varphi) \end{pmatrix}}_{=: \xi} \quad (65)$$

If the yield locus is interpreted as the image of  $\mathbf{x}$  with parameter  $\varphi$  and the constraint  $r = \sigma_y f^{-1/q}$ , a tangential vector can be obtained by deriving with respect to the parameter

$$\mathbf{t} = \frac{\partial \mathbf{x}}{\partial \varphi} = \sigma_y f^{-1/q} \left[ -\frac{f_{,\varphi}}{qf} \xi + \xi_{,\varphi} \right] \quad (66)$$

For plane strain tension,  $\mathbf{t}$  must be strictly vertical, thus  $t_1 = 0$  is required. It follows

$$\frac{f_{,\varphi}}{qf} \xi_1 \Big|_{\varphi=\varphi^{\text{pst}}, \psi=\theta} = \xi_{1,\varphi} \Big|_{\varphi=\varphi^{\text{pst}}, \psi=\theta} \quad (67)$$

and hence

$$f_{,\varphi}(\varphi^{\text{pst}}, \theta) = qf(\varphi^{\text{pst}}, \theta) \frac{\sin(\varphi^{\text{pst}}) + \cos(\varphi^{\text{pst}})}{\sin(\varphi^{\text{pst}}) - \cos(\varphi^{\text{pst}})} \quad (68)$$

### Appendix C. Calibrated Fourier coefficients

**Table C.1**  
Non-trivial coefficients for AA2090,  $q = 6$ .

$a_{0,0}$	$a_{0,4}$	$a_{0,8}$	$a_{1,2}$	$a_{1,6}$	$a_{1,10}$
29.23	60.02	-48.09	-8.019	3.588	-4.387
$a_{2,0}$	$a_{2,4}$	$a_{2,8}$	$a_{3,2}$	$a_{3,6}$	$a_{3,10}$
-33.48	-82.05	68.31	11.67	-5.273	6.24
$a_{4,0}$	$a_{4,4}$	$a_{4,8}$	$a_{5,2}$	$a_{5,6}$	$a_{5,10}$
5.252	23.32	-22.7	-3.651	1.685	-1.854
$a_{6,0}$	$a_{6,4}$	$a_{6,8}$			
-0.188	-1.289	2.474			
$c_{1,0}$	$c_{1,4}$	$c_{1,8}$	$c_{2,2}$	$c_{2,6}$	$c_{2,10}$
-11.72	-138.3	94.89	18.81	-10.1	8.697
$c_{3,0}$	$c_{3,4}$	$c_{3,8}$	$c_{4,2}$	$c_{4,6}$	$c_{4,10}$
3.593	64	-47.53	-12.76	6.92	-5.944
$c_{5,0}$	$c_{5,4}$	$c_{5,8}$	$c_{6,2}$	$c_{6,6}$	$c_{6,10}$
0.1875	-10.74	9.54	2.083	-1.259	1.073

**Table C.2**  
Non-trivial coefficients for AA2008,  $q = 2$ .

$a_{0,0}$	$a_{0,2}$	$a_{0,4}$	$a_{1,0}$	$a_{1,2}$	$a_{1,4}$
1.992	-1.012	0.2548	-0.2422	0.2721	0.05533
$a_{2,0}$	$a_{2,2}$	$a_{2,4}$	$a_{3,0}$	$a_{3,2}$	$a_{3,4}$
-0.6214	1.161	-0.3054	0.3711	-0.2721	-0.05533
$a_{4,0}$	$a_{4,2}$	$a_{4,4}$			
0.06483	-0.1498	0.0506			
$c_{1,0}$	$c_{1,2}$	$c_{1,4}$	$c_{2,0}$	$c_{2,2}$	$c_{2,4}$
0.1798	1.595	-0.3078	0.2403	-0.2742	-0.02055
$c_{3,0}$	$c_{3,2}$	$c_{3,4}$	$c_{4,0}$	$c_{4,2}$	$c_{4,4}$
-0.05992	-0.5315	0.1026	-0.1202	0.1371	0.01028

## References

- [1] R. Hill, A theory of the yielding and plastic flow of anisotropic metals, *Proc. R. Soc. Lond. Ser. A* 193 (1948) 281–297.
- [2] W.F. Hosford, A generalized isotropic yield criterion, *J. Appl. Mech.* 39 (2) (1972) 607–609.
- [3] R. Hill, Theoretical plasticity of textured aggregates, *Math. Proc. Camb. Philos. Soc.* 85 (01) (1979) 179–191.
- [4] R.W. Logan, W.F. Hosford, Upper-bound anisotropic yield locus calculations assuming (111)-pencil glide, *Int. J. Mech. Sci.* 22 (7) (1980) 419–430.
- [5] F. Barlat, O. Richmond, Prediction of tricomponent plane stress yield surfaces and associated flow and failure behavior of strongly textured f.c.c. polycrystalline sheets, *Mater. Sci. Eng.* 95 (1987) 15–29.
- [6] W.F. Hosford, Comments on anisotropic yield criteria, *Int. J. Mech. Sci.* 27 (7) (1985) 423–427.
- [7] F. Barlat, K. Lian, Plastic behavior and stretchability of sheet metals, part I: a yield function for orthotropic sheets under plane stress conditions, *Int. J. Plast.* 5 (1) (1989) 51–66.
- [8] F. Barlat, D.J. Lege, J.C. Brem, A six-component yield function for anisotropic materials, *Int. J. Plast.* 7 (7) (1991) 693–712.
- [9] F. Barlat, J.C. Brem, J.W. Yoon, K. Chung, R.E. Dick, D.J. Lege, F. Pourboghrat, S.H. Choi, E. Chu, Plane stress yield function for aluminum alloy sheets, part 1: theory, *Int. J. Plast.* 19 (9) (2003) 1297–1319.
- [10] F. Bron, J. Besson, A yield function for anisotropic materials application to aluminum alloys, *Int. J. Plast.* 20 (4–5) (2004) 937–963.
- [11] D. Banabic, H. Aretz, D.S. Comsa, L. Paraianu, An improved analytical description of orthotropy in metallic sheets, *Int. J. Plast.* 21 (3) (2005) 493–512.
- [12] F. Barlat, H. Aretz, J.W. Yoon, M.E. Karabin, J.C. Brem, R.E. Dick, Linear transformation-based anisotropic yield functions, *Int. J. Plast.* 21 (5) (2005) 1009–1039.
- [13] G. Ferron, R. Makkouk, J. Morreale, A parametric description of orthotropic plasticity in metal sheets, *Int. J. Plast.* 10 (5) (1994) 431–449.
- [14] H. Vegter, A.H. van den Boogaard, A plane stress yield function for anisotropic sheet material by interpolation of biaxial stress states, *Int. J. Plast.* 22 (3) (2006) 557–580.
- [15] J.W. Yoon, F. Barlat, K. Chung, F. Pourboghrat, D.Y. Yang, Earing predictions based on asymmetric nonquadratic yield function, *Int. J. Plast.* 16 (9) (2000) 1075–1104.
- [16] O. Cazacu, F. Barlat, A criterion for description of anisotropy and yield differential effects in pressure-insensitive metals, *Int. J. Plast.* 20 (11) (2004) 2027–2045.
- [17] O. Cazacu, B. Plunkett, F. Barlat, Orthotropic yield criterion for hexagonal closed packed metals, *Int. J. Plast.* 22 (7) (2006) 1171–1194.
- [18] B. Plunkett, O. Cazacu, F. Barlat, Orthotropic yield criteria for description of the anisotropy in tension and compression of sheet metals, *Int. J. Plast.* 24 (5) (2008) 847–866.
- [19] A.S. Khan, S. Yu, H. Liu, Deformation induced anisotropic responses of Ti-6Al-4V alloy, part II: a strain rate and temperature dependent anisotropic yield criterion, *Int. J. Plast.* 38 (Nov. 2012) 14–26.
- [20] N. Manopulo, C. Raemy, P. Hora, On the modelling of strength differential and anisotropy exhibited by titanium, *J. Phys. Conf. Ser.* 734 (2016) 032051.
- [21] T.B. Stoughton, A non-associated flow rule for sheet metal forming, *Int. J. Plast.* 18 (5–6) (2002) 687–714.
- [22] T.B. Stoughton, J.-W. Yoon, A pressure-sensitive yield criterion under a non-associated flow rule for sheet metal forming, *Int. J. Plast.* 20 (4–5) (2004) 705–731.
- [23] Y. Bai, T. Wierzbicki, A new model of metal plasticity and fracture with pressure and Lode dependence, *Int. J. Plast.* 24 (6) (2008) 1071–1096.
- [24] J.W. Yoon, Y. Lou, J. Yoon, M.V. Glazoff, Asymmetric yield function based on the stress invariants for pressure sensitive metals, *Int. J. Plast.* 56 (2014) 184–202.
- [25] C. Raemy, N. Manopulo, P. Hora, On the modelling of plastic anisotropy, asymmetry and directional hardening of commercially pure titanium: a planar Fourier series based approach, *Int. J. Plast.* 91 (2017) 182–204.
- [26] A. Jeffrey, *Advanced Engineering Mathematics*, 1st edition, Academic Press, San Diego, CA, USA, 2001.
- [27] A. Gray, *Differentialgeometrie: klassische Theorie in moderner Darstellung*, Spektrum Lehrbuch, Spektrum Akademischer Verlag, Heidelberg, Germany, 1994.
- [28] J.C. Simo, T.J.R. Hughes, *Computational Inelasticity*, Springer, 1998.
- [29] C. Raemy, N. Manopulo, P. Hora, A Fourier series based generalized yield surface description for the efficient modelling of orthotropic sheet metals, *J. Phys. Conf. Ser.*, vol. 896, 2017, p. 012016.
- [30] T. Park, K. Chung, Non-associated flow rule with symmetric stiffness modulus for isotropic-kinematic hardening and its application for earing in circular cup drawing, *Int. J. Solids Struct.* 49 (25) (2012) 3582–3593.
- [31] J.W. Yoon, I.S. Song, D.Y. Yang, K. Chung, F. Barlat, Finite element method for sheet forming based on an anisotropic strain-rate potential and the convected coordinate system, *Int. J. Mech. Sci.* 37 (7) (1995) 733–752.